Available online at www.sciencedirect.com

ScienceDirect

Procedia Structural Integrity 2 (2016) 3684–3696

Structural Integrity Procedia

www.elsevier.com/locate/procedia

21st European Conference on Fracture, ECF21, 20-24 June 2016, Catania, Italy

A new yield criteria including the effect of lode angle and stress triaxiality

G. Mirone[a]*, R. Barbagallo[a], D. Corallo[a]

[a]*University of Catania, Dept. of Industrial Engineering, Viale A. Doria 6, 95125, Catania, Italy*

Abstract

According to several experiments reported in the literature, the elastoplastic behaviour of metals depends not only on the first stress invariant (triaxiality) for the ductile damage and on the second stress invariant (equivalent von Mises stress) for the yield, but also on the third stress invariant (normalized Lode angle X) which may affect at the same time the yielding and the ductile failure.

In this paper a new yield model is presented, where the yield surface depends on the Lode Angle and, eventually, also on the triaxiality ratio.

The proposed model is identified by a calibration parameter expressing the degree of nonlinearity of the yield with respect to the Lode angle, and a calibration function expressing the maximum variability of the hardening stress at the two extremities of the Lode angle range, corresponding to the uniaxial and to the pure shear stress states.

The proposed model has been tested against several experimental data from the literature on the Titanium alloy Ti6Al4V, including mixed tension-torsion loading which allowed to control the evolution of X and to confine its values into different narrow ranges for better investigating the Lode angle effects on the yield response.

Peer-review under responsibility of the Scientific Committee of ECF21.

Keywords: Yield stress, elastoplastic hardening, triaxiality, Lode angle

* Corresponding author. Tel.: +39-95-7382418; fax: +39-95-330258.
E-mail address: gmirone@dii.unict.it

Peer review under responsibility of the Scientific Committee of ECF21.
10.1016/j.prostr.2016.06.458

1. Introduction

For completely describing the local stress state at single material points of loaded structures, three parameters are necessary, namely, the principal stresses or the invariants of the stress tensor.

In the classical plasticity framework, the second deviatoric stress invariant is assumed to be sufficient for describing the elastoplastic response of structural materials via the von Mises criteria and the hardening functions, the first expressing the yield condition through a yield surface in the stress space, the second relating the evolving size of such a surface to the equivalent plastic strain.

Frequently, the response of structural metals does not comply with such idealization because also the stress triaxiality TF (first stress invariant normalized to the Mises stress) and the normalized Lode angle X (based on the third stress invariant normalized by the Mises stress) play a significant role on the elastoplastic response and on the ductile fracture.

Since the sixties of the past century, the stress triaxiality is known to accelerate the failure of ductile materials by decreasing their failure strain (Chaboche (1988), Lemaitre (1985), Mackenzie et al. (1988), McClintock (1968), Rice and Tracey (1969), Gurson (1977), Tvergaard and Needleman (1984), Barsoum and Faleskog (2007), Mashayekhi and Ziaei-Rad (2006), Bai and Wierzbicki (2010), Xue and Wierzbicki (2009)); this aspect is completely ascertained and many models are available in the literature (Bao and Wierzbicki (2004), Brunig et al. (2008), Mirone (2004), Wierzbicki et al. (2005)), although no triaxiality-related failure criteria is still universally accepted.

Similar considerations apply to the third invariant expressed by normalized Lode angle, whose role in the embrittlement of materials is gaining stronger evidence in the recent years (Xue (2009), Xue et al. (2010), Mae et al. (2007), Ghajar et al. (2013), Mirone and Corallo (2010), Graham et al. (2012), Barsoum et al. (2012), Faleskog et al. (2013), Xue et al. (2013), Papasidero et al. (2014), Rodríguez-Millán (2015), Cortese et al. (2014)) but is not yet fully recognized.

Also the elastoplastic response of structural materials is potentially affected by the triaxiality factor TF and by the deviatoric parameter X; the triaxiality is known to directly influence the plastic yield of granular materials, ceramics etc., but at the same time it seems to have a negligible effect on the plasticity of most metals (Bigoni and Piccolroaz (2004), Piccolroaz and Bigoni (2009), Penasa et al. (2014), Lehmann (1985)), suggesting that their yield surface in the stress space has constant cross section along the trisector axis.

Conversely, the deviatoric parameter X is found to play a key role on the yield of many metals; in such cases, the flow curves from tension may significantly differ from those obtained by torsion (Bai and Wierzbicki (2008), Erice and Gálvez (2014), Gao et al. (2009), Gao et al. (2011), Dorogoy et al. (2015), Cortese et al. (2015), Mirone (2014)), although it is not a generalized occurrence, and the stress-strain plastic response of other metals is almost unaffected by X (autori yield surface cilindrica).

Then the yield surface of metals may either have a circular, Mises-like cross section or as a six-lobed, Lode-angle dependent cross section. In case of anisotropic metals with X-dependent yield, also the six-lobed symmetry does not apply and a full dependence of the yield stress on the Lode angle occurs on a 360 degrees domain, for each given hardening state of the material.

In this paper, a new yield model including a dependence on both the TF and X is proposed, including the functions by von Mises and by Tresca as special cases of full insensitivity and of reference sensitivity to X, respectively.

Experimental data from the literature including mixed tension/torsion tests are used for assessing the predictive capability of the yield model by way of fortran subroutines implemented in finite element simulations of the experiments.

2. Yield Model formulation and calibration

A given stress tensor corresponds to a point in the space of principal stresses and can be either identified by the Cartesian coordinates s1, s2, s3 in a rectangular reference system or by the Haigh coordinates in a cylindrical reference system; the stress coordinates also express the three invariants of the stress tensor which can be combined each other in the following parameters:

$$\sigma_{Mises} = \sqrt{\frac{1}{2}\left[(\sigma_1 - \sigma_2)^2 + (\sigma_3 - \sigma_2)^2 + (\sigma_1 - \sigma_3)^2\right]} \tag{1}$$

$$X = Sin(3 \cdot \vartheta) = \frac{27}{2} \cdot \frac{(\sigma_1 - \sigma_H) \cdot (\sigma_2 - \sigma_H) \cdot (\sigma_3 - \sigma_H)}{\sigma_{eq}{}^3} \tag{2}$$

$$TF = \frac{\sigma_H}{\sigma_{eq}} = \frac{\sigma_1 + \sigma_2 + \sigma_3}{3 \cdot \sigma_{eq}} \tag{3}$$

where $\sqrt{2/3} \cdot \sigma_{Mises}$ is the radial coordinate of the stress state (Figure 1) based on the second stress invariant, the deviatoric parameter X is the Lode angle θ (third invariant of deviatoric stress) normalized over +/- 30 deg intervals, and the triaxiality factor TF expresses the axial coordinate (related to the first stress invariant and to the hydrostatic stress σ_H), normalized to the equivalent stress.

Considering that isotropy is assumed to apply, the Yield Surface (YS) has a tri-lobe symmetry around the {1, 1, 1} axis. In case of positive-negative symmetry (yield stresses in tension and compression identical each other), then a six-lobed symmetry applies.

The greatest possible evidence of the Lode angle affecting the yield of some materials is given by the difference found between the hardening curves in pure tension and in pure torsion.

The phenomenological YS proposed here is a combination of the von Mises and the Tresca surfaces, based on a Tresca-like linear cross section with straight edges connecting the pure shear and the purely uniaxial yield conditions, over which a tunable amplification is superimposed in the form of a quadratic function of the Lode angle, ensuring a flexible calibration parameter with good control of the convexity of the yield surface.

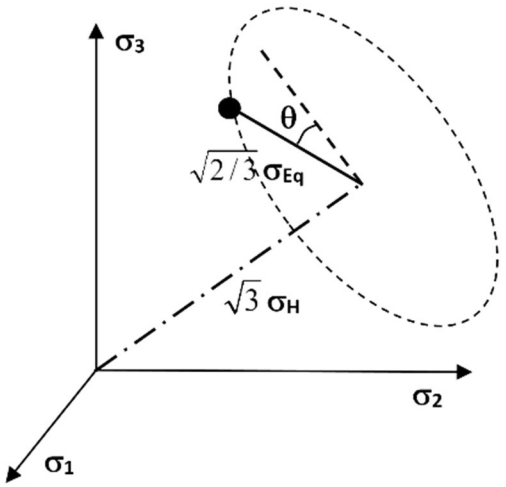

Figure 1 Cylindrical, stress invariants-based coordinates

As usual for metals, the effect of the triaxiality on the yield surface is supposed to be negligible, then the yield surface has a uniform cross section along the trisector axis, and the whole surface can be then identified by its intersection with the deviatoric plane. However, a tapered cross section modelling the effect of hydrostatic pressure on the yield can be easily included as in Mirone (2014).

Assuming symmetrical behaviours in tension and compression the definition of the yield surface can be limited to the interval of Lode angles [0,30].

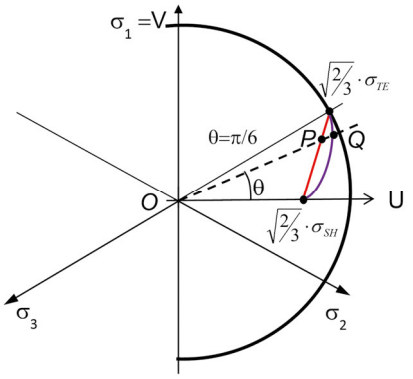

Figure 2: yield surface edge definition

According to the scheme of Figure 2, a Cartesian reference U-V is assumed on the deviatoric plane, so that the U axis identifies a zero Lode angle, pure shear direction. The red line identifies a Tresca-like yield surface with straight edges accounting for a Lode-angle dependent yield stress, spanning between σ_{TE} in pure tension and σ_{SH} in pure shear.
Such a segment is described by the equation of a line passing across the above points on the deviatoric plane:

$$V = \frac{1}{m}\cdot\left(U - \sqrt{\frac{2}{3}}\cdot\sigma_{SH}\right); \quad m = \frac{\sigma_{TE}\cdot\cos(\pi/6) - \sigma_{SH}}{\sigma_{TE}\cdot\sin(\pi/6)} \tag{4}$$

The intersection *P* between such segment and the general direction at Lode angle θ can be then easily found, and its distance from the origin returns the current yield stress according to the straight-edged yield surface connecting the pure shear and the uniaxial yield stresses:

$$\overline{OP}(\vartheta) = \sqrt{{U_p}^2 + {V_p}^2} = \sqrt{\frac{2}{3}}\cdot\sigma_{SH}\cdot\frac{\sqrt{1+\tan^2(\vartheta)}}{1 - m\cdot\tan(\vartheta)} \tag{5}$$

Then, a Lode angle-dependent quadratic amplification of the yield stress is introduced for better flexibility as a second order multiplicative term, whose effect is qualitatively depicted by the blue curve in Figure 2. Such a quadratic amplification spans from 1.0 at the extremities of the Lode angle range (θ=0 and θ=π/6), up to the desired calibration value at the desired representative angle θ*, so providing a single calibration parameter. As far as the calibration value is positive, the resulting yield surface is convex in the Lode angle range (0, π/3), which is where convexity must be ensured.
The radial coordinate of the point Q is then obtained by incrementing that of the point P by the above quadratic term, and the equivalent stress is finally defined as in equation 6.

$$\sigma_{Eq}(\vartheta) = \sqrt{\frac{3}{2}}\cdot\overline{OQ}(\vartheta) = \sigma_{SH}\cdot\frac{\sqrt{1+\tan^2(\vartheta)}}{1 - m\cdot\tan(\vartheta)}\cdot\left[1 + qa\cdot\frac{\left(\vartheta^2 - \pi/6\cdot\vartheta\right)}{\vartheta^{*2} - \pi/6\cdot\vartheta^*}\right] \tag{6}$$

where *qa* is the only calibration parameter, required together with the *m* function, for assessing the quadratic amplification of the yield due to the Lode angle, and for finalizing the current shape of the yield surface.
The hardening effect in equation (6) is provided by the evolving scale factor σ_{Sh}, which is the current, strain-dependent yield stress in pure shear, while the possible variability of the surface shape during the straining process is included in the term *m*, which expresses the strain-dependent relationship between the hardening stresses under pure uniaxiality and pure shear. The degree of curvature of the surface edges is instead assumed to be constant as the

parameter *qa*, so far, is assumed to be a strain-independent material constant.
Then the yield surface can be also expressed in the fully equivalent form of eq. 7, where the hardening is accounted for by the more familiar hardening stress in pure tension σ_{Te}, playing the role of the evolving, strain-dependent scale factor:

$$\sigma_{Eq}(\vartheta)=\sigma_{TE}\cdot\left(\cos\left(\frac{\pi}{6}\right)-m\cdot\sin\left(\frac{\pi}{6}\right)\right)\cdot\frac{\sqrt{1+\tan^2(\vartheta)}}{1-m\cdot\tan(\vartheta)}\cdot\left[1+qa\cdot\frac{\left(\vartheta^2-\mu/6\cdot\vartheta\right)}{\vartheta^{*2}-\mu/6\cdot\vartheta^*}\right] \tag{7}$$

In principle, the complete identification of such a yield surface can be made by two base experiments in pure tension and in pure torsion, providing the hardening stresses (σ_{TE} σ_{SH} and m), plus one more single test at the intermediate Lode angle θ^*, for calibrating the additional parameter *qa*.
More reasonably, the parameter *qa* can be found by minimizing the discrepancies of finite elements runs against a finite set of tests at intermediate Lode angles.
If *m=atan(15 deg)*, then the parameter *qa* can be tuned for making the yield surface to collapse on the Mises surface, depending on the arbitrary calibration angle θ^*. If instead *m=0* and *q=0* , the Tresca surface is obtained as a special case.
The variability of *qa* with the plastic strain can be eventually introduced, making it a calibration function instead of a calibration constant, so allowing to model further strain-promoted shape evolutions of the yield surface and then giving one more degree of flexibility to the proposed Yield model.
Figure 3 shows four possible yield surfaces for a given reference uniaxial yield stress, where the shear yield stress is greater or smaller than the Tresca yield stress (outward or inward protruding dodecagons) and the quadratic amplification is either turned off or is imposed to be 20% at 15 deg (straight or curved edges).

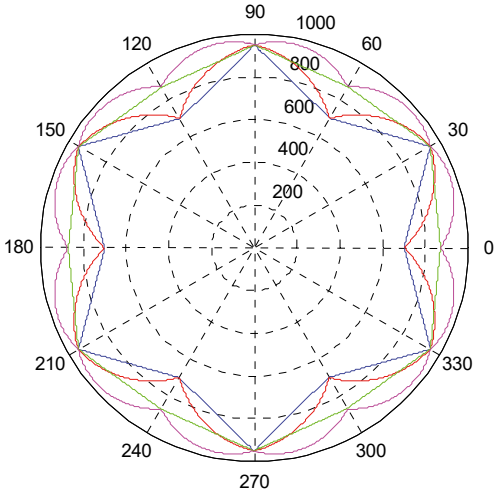

Figure 3: Four different Yield surfaces corresponding to a given uniaxial stress and two couples of shear stress / quadratic amplification.

3. Experiments and Lode angle -dependent yield calibration

The yield model discussed here is checked against literature experimental data on Ti6Al4V by Allahverdizadeh, Nima, et al. (2015).
The above experimental campaign includes pure tension, pure torsion and mixed tension-torsion tests imposed by a constant tensile preload followed by monotonically increasing torque up to failure, so that the deviatoric parameter can be virtually controlled at the local scale for investigating its effect on the stress-strain response.
In fact, axisymmetric tensile stress states (including uniaxiality as special case) generates X=1, while the generalized plane strain (including pure torsion as special case) makes X=0; mixing both load types in the desired proportions allows to determine and maintain the desired values of X at the meaningful material points within the specimens.

Table 1. Experimental tests by Allahverdizadeh et al.

Material	Series id	Test type	Specimen shape
Ti6Al4V Allahverdizadeh et al.	ATo	Torsion	“
	A20	pre-Tension 20 kN + Torsion	“
	A30	pre-Tension 30 kN + Torsion	“
	A40	pre-Tension 40 kN + Torsion	“
	TFS	Tension	Tens. Flat smooth
	SFB	Shear	Shear Flat butterfly
	TFH	Tension	Tens. Flat holed
	TFN	Tension	Tens. Flat notch. R 6.67
	TRS	Tension	Tens. Round smooth
	TRN	Tension	Tens. Round Notched
	TPB	Three-points Bending	Notched square bar

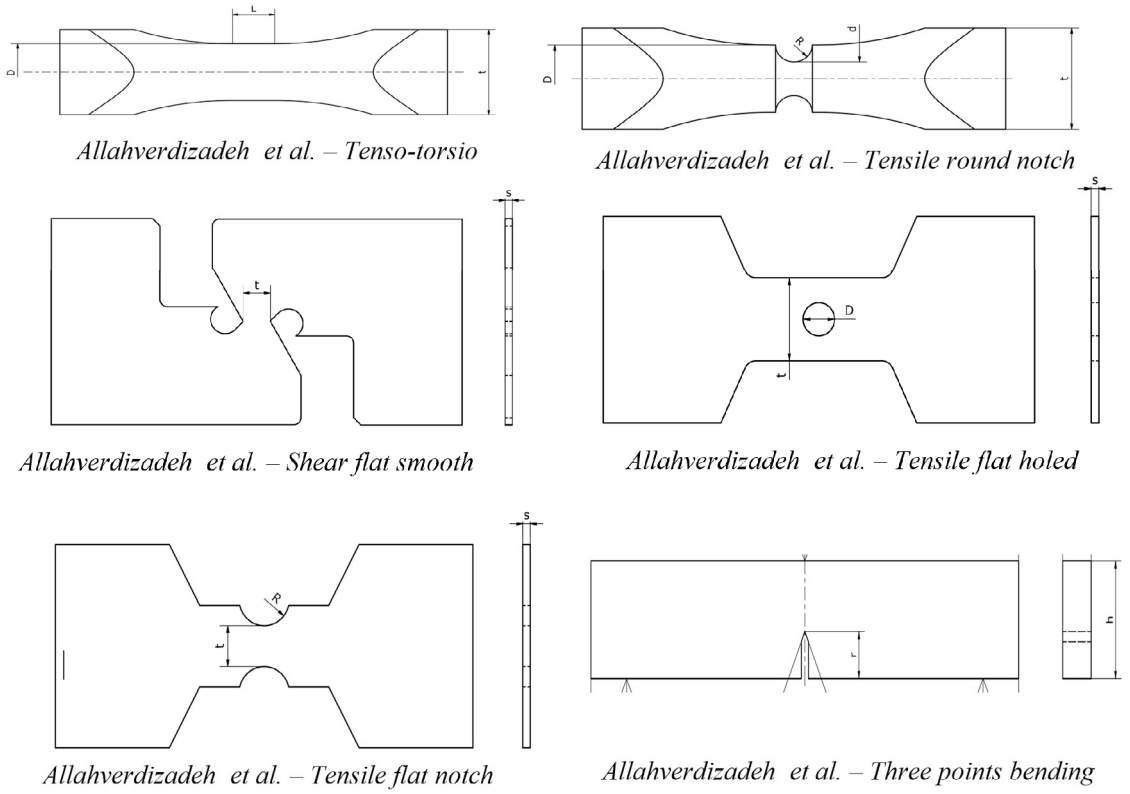

Figure 4: Specimens shapes and load modes

In Table 1 are identified the tests from literature (Allahverdizadeh et al (2015)) used here for checking the accuracy of the proposed yield model.

Also flat specimens with butterfly-like, grooved and notched shapes are included in the test series according to Figure 4, providing further data about particular combinations of evolving X and TF values.

The reader may refer to Allahverdizadeh et al. (2014), Allahverdizadeh et al. (2015) and Allahverdizadeh PhD Thesis (2014) for further details about the experiments.

For the Ti alloy considered here, the load-elongation-diameter curves and the specimens geometry data reported in

Allahverdizadeh et al. (2014), Allahverdizadeh et al. (2015) and Allahverdizadeh PhD Thesis (2014) allow the derivation of the tensile flow curve including the postnecking correction (e.g. reverse engineering, Bridgman, MLR), while the flow curve in torsion is obtained from the torque-angle experimental data processed through the Nadai torsional formulation (Nadai (1963)), respectively.
The material hardening functions from tensile and from torsional tests after a general reassessment of the data are summarized in Table 2 and plotted in *Figure 5*.

Table 2. Material hardening functions in tension and torsion

Material	Test type	Flow curves
Ti6Al4V Allahverdizadeh et al.	Tension	$\sigma_{Eq-Tens} = 1335 \cdot \varepsilon_{Eq}^{0.06}$ (pre-necking)
		$\sigma_{Eq-Tens} = 1058 + 1230 \cdot \varepsilon_{Eq} - 550 \cdot \varepsilon_{Eq}^{2}$ (post-necking)
	Torsion	$\sigma_{Eq-Tors} = 1325 \cdot \varepsilon_{Eq}^{0.08}$

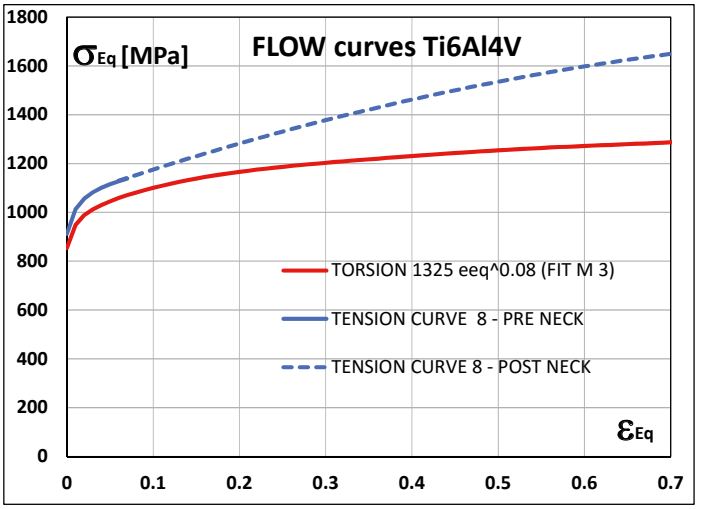

Figure 5: Material hardening functions in tension and torsion

The significant departure of the flow curve in torsion from that in tension evidences that the Lode angle plays a key role in the yield of this metal.
The evolving function $m(\varepsilon_{Eq})$ for the Ti6Al4V alloy, derived according to the yield model proposed here and to eq. (4), is plotted in *Figure 6*.
The initial negative values of m indicate that, at the beginning of the plastic range, the yield stress in pure shear is intermediate between the Tresca one and the Mises one at the given hardening level.
The increasing values of m imply that the shape of the cross sections of the yield surface progressively changes, and the small protrusion it shows just after the first yield at the pure shear angular coodinate, tends to move inward and becomes less and less pronounced as the plastic strain evolves.
When $m=0$ the yield in pure shear becomes identical to that of the classical Tresca criteria, although the yield stress at different Lode angles is generally beyond the Tresca prediction; if instead also the quadratic parameter $qa=0$, then the whole surface collapses into the Tresca one.
Positive values of m indicate that the yield surface exhibits inward edges at the zero Lode angle and the yield stress in pure shear is lower than the Tresca prediction at that hardening level.

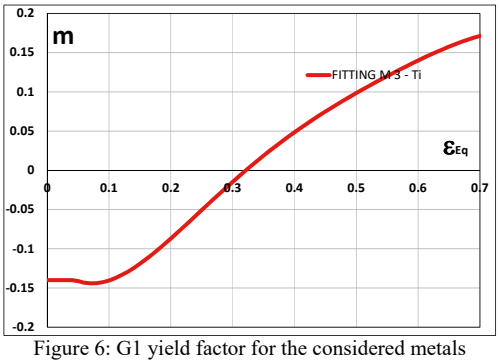

Figure 6: G1 yield factor for the considered metals

The second yield parameter of the yield model, *qa*, is calibrated by finite elements-based reverse engineering, as a compromise allowing to satisfactorily reproduce the macroscopic response (load-elongation and torque-angle curves) of the various mixed tension-torsion tests performed at different combinations of such loading modes.
All the finite elements analyses are based on the update Lagrangian finite general plasticity with additive decomposition of the strains, available in a commercial nonlinear code; the proposed yield critieria and the corresponding associative plasticity are implemented via fortran user subroutines. The tension-torsion displacements are imposed via contact surfaces where the proper constraints, motions and loads are imposed (see *Figure 7*).

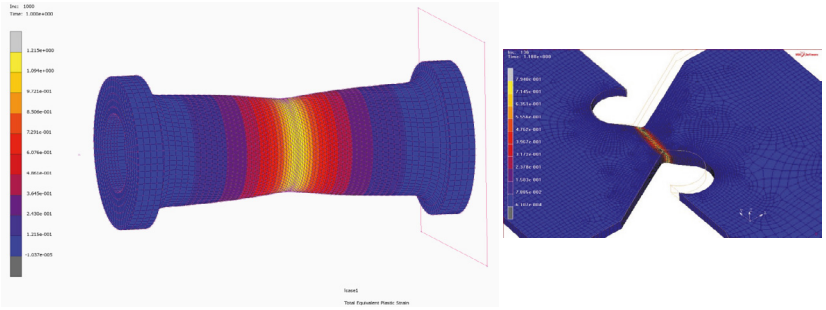
Figure 7: Deformed meshes of tension-torsion and flat shear specimens

The value attributed to the *qa* parameter for the Ti6Al4V is 0.043 and, together with the *m* function in *Figure 6* and the uniaxial hardening function in Figure 5, generates the expanding yield surfaces reported in *Figure 8* at the strain levels of 0.02, 0.2, 0.4, 0.6, respectively.

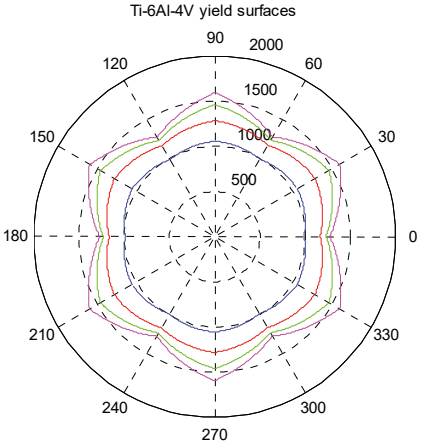

Figure 8: Evolving yield surface of the Ti-6Al-4V alloy at different strain levels

The yield surface changes its shape during the straining history, but the degree of curvature of its cross section edges is fixed because of the constant value of *qa.* An upgrade of the model is in progress for making the quadratic amplification *qa* variable with the plastic strain, increasing the model flexibility.
The results of the finite elements runs performed with the proposed yield model and with the standard Mises yield criteria are presented in the next section for the various tests by Allahverdizadeh et al.; the data are presented in terms of macroscopical response parameters like load, elongation, torque and twist angle.

4. X-dependent yield and numerical simulations

In *Figure 9* the experimental results are compared to the predictions of the proposed yield criteria (plots A and C) and to the outcome of finite elements with standard Mises plasticity (plots B and D).
The most iportant outcome of a Lode angle-dependent yield surface is the differentiation of the evolving yield stress under pure tension from that under pure shear; with this regard the proposed model (black continuous curve in *Figure 9 C*) allows to reproduce very well the experimental data with almost no error (large filled black dots in *Figure 9 C* and *D*), while the standard von Mises predictions, typically based on the flow curves from tension, (black dashed line in *Figure 9 D*) generate considerable approximations in simulating the torsion experiments with an error close to 15% at failure.

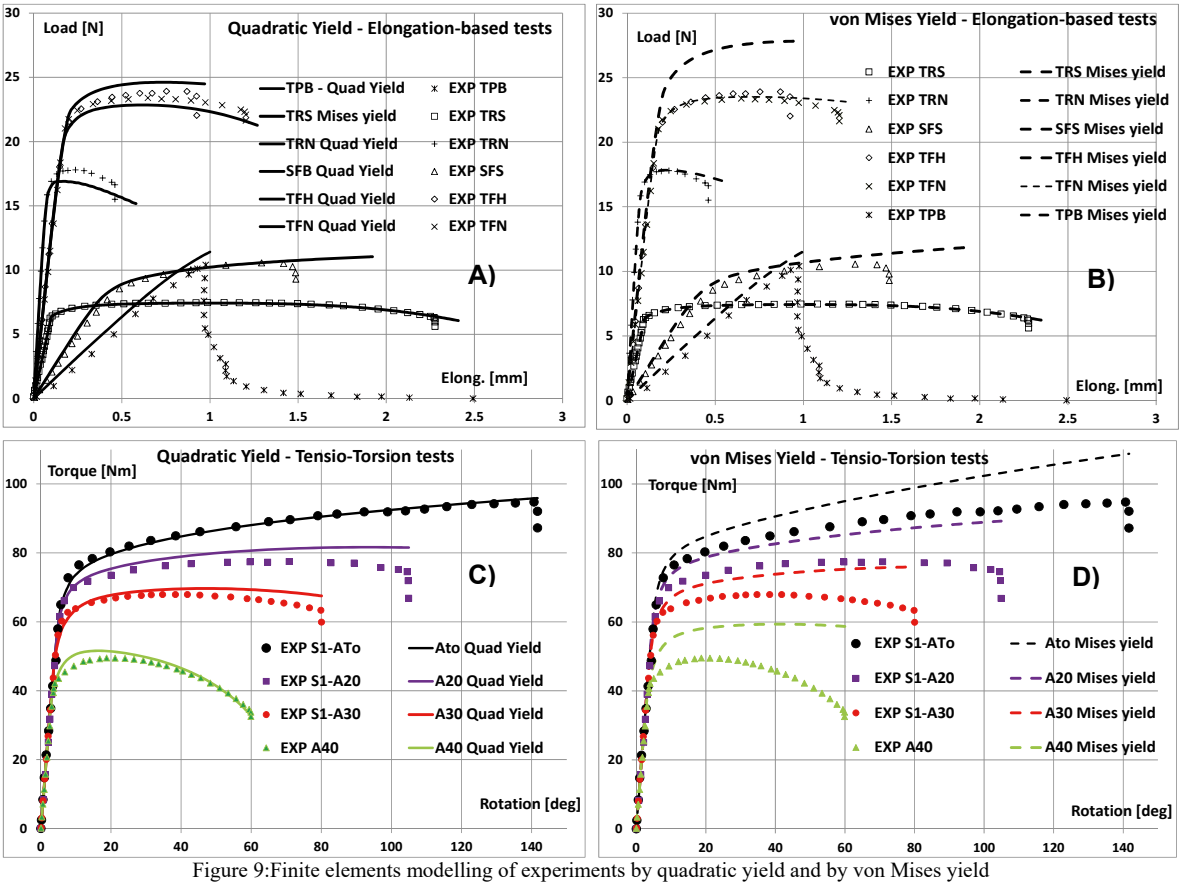

Figure 9:Finite elements modelling of experiments by quadratic yield and by von Mises yield

The data in *Figure 9 A* and *B* refer to the extension-based tests where, although shear stress at the local scale can be generated due to finite straining, no macroscopical twist nor torque are applied; here no color code is used for differentiating the curves of the various tests, as the relationship between an experimental set and the corresponding finite element simulation is clearly identified.

All the tests of this series are simulated reasonably by the Mises yield and no great improving is introduced by using the quadratic yield, except for the "tensile flat holed" test, TFH, where the poor accuracy provided by the Mises yield (error beyond 12% at failure) is substantially fixed by the proposed yield model (error close to 3% at failure).
Instead, the data in in *Figure 9 C* and *D,* for the mixed tension-torsion tests, include a color coding other than the curves symbols, because the Mises-based numerical simulations exhibit such a poor approximation that the curves from a certain simulated test are close to the experimental data from a different test, and the correspondence of the numerical curves to the experimental ones is not always clear.
The error at failure of the tensio-torsion simulations based on the Mises yield spans from 15% (pure torsion) to 30% (A40 tests).
Such a discrepancy cannot be due to the damage, affecting the experiments and not modeled by the finite elements. In fact, the progressive microvoid evolution in tension-dominating stress states is known to play negligible role on the value of the local stresses and of the macroscopic load, as confirmed by the good accuracy of the Mises-based finite elements fot the elongation-based tests of Figure 9 A and B. Instead in Figure 9 C and D, the 15% error of the pure torsion, increases up to 30% for the test A40 where the axial component of the stress state is the greater of the lot.
Then, such a poor accuracy of the simulations with Lode angle deviating from 30 degs. can be reasonably attributed to the whole Mises yield criteria alone, and the adoption of the quadratic-yield formulation proposed here is capable of largely reducing the error, which drops down to the range between almost zero (pure torsion) and 8% (A20 test), with no apparent dependence on the mix between tension and torsion.
The stress paths for the A20 and A40 tension-torsion tests at the most meaningful material points in the specimens (mid-thickness and outer surface at the neck section) are acquired from the finite elements runs with the X-dependent yield, and are reported in *Figure 10* for the "extreme" mixed tests A20 and A40.

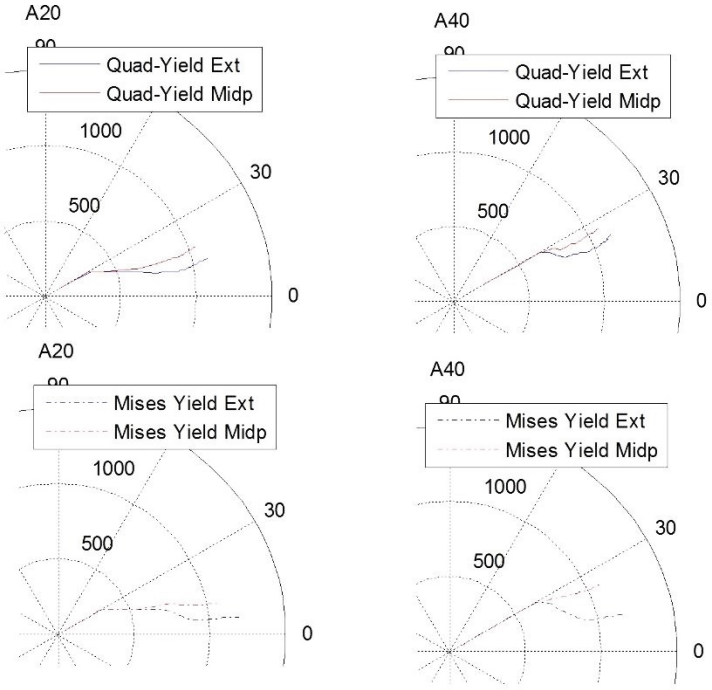

Figure 10: Stress histories of A20 and A40 tests at critical material points

The stress paths are initially very close to the pure tension because of the tensile preload, then the A20 test quickly departs from uniaxiality after yield because of the low preload, instead the A40 test where the tensile preload is greater, only later departs from uniaxiality, closer to the first yield condition.
In both cases the paths tend to deviate from their initial straight trajectory, converging toward intermediate stress states at higher plastic strains.

As expectable, the larger deviations from uniaxiality occur in the A20 test because the evolving ratio between the torque and the low-level tensile preload is greater than it is in the A40 test.
In both tests, the stress paths of the material points on the outer surface of the specimens deviate from uniaxiality more than the inner ones, because the torque-induced shear stress is null at the specimen core and increases along the section radius toward the secimens surface.
The points on the specimen axis, not reported in *Figure 10*, are subjected to the tensile preload alone, so their stress path evolves along the 30 deg direction until failure.

The adoption of the quadratic yield also implies minor modifications of the stress paths, by reducing the variation of the Lode angle between the beginning and the end of each test, as visible by comparing the upper solid line plots of *Figure 10* to the lower ones.
Summarizing, it is possible to say that the greater departure of the experimental evidence from the Mises criteria, occurring under pure shear conditions, is reproduced very well by the new yield criteria proposed here; this means that the *m*-based feature of the model is capable of correctly reproducing virtually whatever possible departure function of the pure torsion hardening from the purely tensile hardening.
The *qa*-based feature which determines the model transition from pure tension to pure shear at intermediate values of the deviatoric parameter might require further adjustments and upgrades.
The single-valued constant *qa* resulted to be suitable for correctly modeling the response of the Ti6Al4V alloy but, for different materials, it is very likely that a strain-dependent variable curvature of the edges of the yield surface must be implemented through a multi-valued *qa* function of the strain.

5. Conclusions

A new yield criteria is developed here, based on the experimental evidence that many structural metals exhibit different hardening functions when the plastic deformation occurs under differently evolving Lode angles.
The proposed yield surface is initially based on a blend of the von Mises surface to a Tresca-like one, with dodecagonal straight-edged cross section.
Such yield function, X-dependent through the calibrating term *m* which expresses the relationship between the hardenings in pure shear and in pure tension, is further amplified by a quadratic function of the Lode angle calibrated through the material constant *qa*. Eventually, a similar dependence on the hydrostatic stress can be added for including the effect of the stress triaxiality, if the material response requires it.
Experimental data by Allahverdizadeh et al. on Ti6Al4V are used for calibrating the model and for checking its suitability to reproduce the behavior of such alloy undergoing various plastic straining histories, occurring under different stress paths and Lode angle ranges.
The experimental variability of the Lode angle is provided through assorted mixes of tension-torsion, pure tension and pure torsion, as well as by pulling tests of flat plane strain and shear butterfly-like specimens.
The calibrated model allows to reproduce all the experiments with good accuracy, leaving almost unaltered the already good accuracy shown by the classical Mises plasticity for the tests where the stress states evolve closer to uniaxiality, while almost completely fixing the substantial error which the same Mises plasticity introduces when the simulated tests involve variable Lode angles departing from uniaxiality.
Further experiments, generating constant Lode angles and scanning the 0-30 degrees range in finer intervals, might be useful for better assessing the sensitivity of the yield to Lode angle variations.
Although the elastoplastic response of the Ti6Al4V alloy is accurately modeled by the proposed yield function, other materials should be modeled for checking the model generality, eventually including an upgrade of the yield model currently in progress, which incorporates a strain-dependent quadratic amplification parameter $qa((\varepsilon_{EQ})$.

References

Allahverdizadeh N., A. Manes, M. Giglio, A. Gilioli, 2014.Geometry Transferability of Lemaitre's Continuum Damage Mechanics Model in the Plane Stress Specimens, Key Engineering Materials, 592-593, 266-270, 2014

Allahverdizadeh N.,, 2014. PhD Thesis, Polithecnic of Milan.
https://www.google.it/url?sa=t&rct=j&q=&esrc=s&source=web&cd=1&ved=0ahUKEwic2LPo76HMAhVoLcAKHVmkBooQFggeMAA&ur

l=https%3A%2F%2Fwww.politesi.polimi.it%2Fbitstream%2F10589%2F89287%2F1%2FNima%2520Allahverdizadeh.pdf&usg=AFQjCNE TtNj9ct4EPXC0Zs9D18hcK7gbHg&bvm=bv.119745492,d.bGg&cad=rja

.Allahverdizadeh, 2015. An experimental and numerical study for the damage characterization of a Ti–6AL–4V titanium alloy. International Journal of Mechanical Sciences 93, 32-47.

Bai Y, Wierzbicki T., 2008. A new model of metal plasticity and fracture with pressure and Lode dependence, International Journal of Plasticity 24, 1071–1096.

Bai, Y., Wierzbicki, T., 2010. Application of extended Mohr–Coulomb criterion to ductile fracture, Int J Fract 161, 1–20

Bao, Y., Wierzbicki, T., 2004. On fracture locus in the equivalent strain and stress triaxiality space. Int. J. Mech. Sci. 46, 81–98.

Barsoum I., Faleskog J., 2007. Rupture mechanisms in combined tension and shear—Experiments, International Journal of Solids and Structures 44, 1768–1786.

Barsoum, Imad, Jonas Faleskog, Shivinandan Pingle, 2012. The effect of stress state on ductility in the moderate stress triaxiality regime of medium and high strength steels. International Journal of Mechanical Sciences 65.1, 203-212.

Bigoni D., Piccolroaz A., 2004. Yield criteria for quasibrittle and frictional materials, International Journal of Solids and Structures 41, 2855–2878.

Brunig M., Chyra O., Albrecht D., Driemeier L., Alves M., 2008. A ductile damage criterion at various stress triaxialities, International Journal of Plasticity, 24 (2008) 1731–1755.

Chaboche, JL., 1988. Continuum damage mechanics, Part I and II. J. Appl. Mech. 5 (55), 59–72.

Cortese, L., Coppola, T., Campanelli, F., Campana, F., Sasso, M. (2014). Prediction of ductile failure in materials for onshore and offshore pipeline applications. International Journal of Damage Mechanics, 23(1), 104-123.

Cortese L., 2015. A J2–J3 approach in plastic and damage description of ductile materials. International Journal of Damage Mechanics, 1056789515577228.

Dorogoy, A., Rittel, D., Godinger, A., 2015. A Shear-Tension Specimen for Large Strain Testing Experimental Mechanics, 1-13

Erice E., Gálvez F., 2014. A coupled elastoplastic-damage constitutive model with Lode angle dependent failure criterion, International Journal of Solids and Structures 51, 93–110.

Faleskog, Jonas, Imad Barsoum, 2013. Tension–torsion fracture experiments—Part I: Experiments and a procedure to evaluate the equivalent plastic strain. International Journal of Solids and Structures 50.25, 4241-4257.

Gao X. Zhang T., Hayden M., Roe C., 2009. Effects of the stress state on plasticity and ductile failure of an aluminum 5083 alloy, International Journal of Plasticity 25, 2366–2382.

Gao X., Zhang T., Zhou J., Graham S., Hayden M., Roe C., 2011. On stress-state dependent plasticity modeling: Significance of the hydrostatic stress, the third invariant of stress deviator and the non-associated flow rule, International Journal of Plasticity 27, 217–231.

Ghajar R., Mirone G., Keshavarz A, 2013. Sensitivity Analysis on triaxiality factor and Lode angle in ductile fracture, Journal of Mechanics, 29, 177-184.

Graham S., Zhang T., Gao X., Hayden M., 2012. Development of a combined tension–torsion experiment for calibration of ductile fracture models under conditions of low triaxiality, International Journal of Mechanical Sciences 54, 172–181.

Gurson, A.L., 1977. Continuum theory of ductile rupture by void nucleation and growth. ASME Trans. J. Eng. Mater. Technol. (99), 2–15.

Lemaitre, J., 1985. A continuous damage mechanics model for ductile fracture. J. Eng. Mater. Technol. (107), 83–99.

Lehmann Th., 1985. On a Generalized Constitutive Law in Thermo-Plasticity Taking into Account Different Yield Mechanisms* Aeta Mechaniea 57, 1-23.

Mackenzie, A.C., Hancock, J.W., Brown, D.K., 1977. On the influence of state of stress on ductile failure initiation in high strength steels. Eng. Fract. Mech. (9), 167–188.

Mae, H., Teng, X., Bai, Y., Wierzbicki, T., 2007. Calibration of ductile fracture properties of a cast aluminum alloy, Materials Science and Engineering A 459, 156–166.

Mashayekhi, M., Ziaei-Rad, S., 2006. Identification and validation of a ductile damage model for A533 steel, Journal of Materials Processing Technology 177, 291–295.

McClintock, F.A., 1968. A criterion for ductile fracture by growth of holes. J. Appl. Mech. (35), 363–379.

Mirone, G., 2004. Approximate model of the necking behaviour and application to the void growth prediction, Int. J. of Damage Mechanics 13 (3), 241-261.

Mirone G., Corallo D., 2010. a local viewpoint for evaluating the influence of stress triaxiality and lode angle on ductile damage and hardening, International Journal of Plasticity 26, 348–371.

Mirone, G., 2014. Effetto Dei Parametri Di Triassialità e Deviatoricità sulla Risposta Dei Materiali Duttili. AIAS.

Nadai, A., 1963. Theory of flow and fracture solids - Volume 2. McGraw Hill, New York.

Papasidero, J., Doquet, V., Mohr, D., 2014. Determination of the effect of stress state on the onset of ductile fracture through tension-torsion experiments. Experimental Mechanics 54.2, 137-151.

Paul, B., 1968. Generalized pyramidal fracture and yield criteria , Int. J. Solids Strucrures 4, 175 - 196.

Penasa, M., Piccolroaz, A., Argani, L., Bigoni, D., 2014. Integration algorithms of elastoplasticity for ceramic powder compaction , Journal of the European Ceramic Society 34, 2775–2788

Piccolroaz, A., Bigoni, D., 2009. Yield criteria for quasibrittle and frictional materials: A generalization to surfaces with corners International Journal of Solids and Structures 46, 3587–3596

Rice, J.R., Tracey, D.M., 1969. On the ductile enlargement of voids in triaxial stress fields. J. Mech. Phys. Solids 17, 201–217.

Rodríguez-Millán, M., Vaz-Romero, Á., Arias, Á., 2015. Failure behavior of 2024-T3 aluminum under tension-torsion conditions. Journal of Mechanical Science and Technology 29.11, 4657-4663.

Tvergaard, V., Needleman, A., 1984. Analysis of the cup-cone fracture in a round tensile bar. Acta Metall. 32 (1), 157–169.

Wierzbicki, T., Bao, Y., Lee, Y.-W., Bai, Y., 2005. Calibration and evaluation of seven fracture models. Int. J. Mech. Sci. 47, 719–743.

Xue, L., 2009. Stress based fracture envelope for damage plastic solids Engineering Fracture Mechanics 76, 419–438

Xue, L., Wierzbicki, T., 2009. Ductile fracture characterization of aluminum alloy 2024-t351 using damage plasticity theory, International Journal of Applied Mechanics, 1(2), 267–304.

Xue, Z., Pontin M.G., Zok F.W., Hutchinson J.W.. 2010. Calibration procedures for a computational model of ductile fracture. Engineering Fracture Mechanics 77.3, 492-509

Xue, Z., Faleskog, J., Hutchinson, J. W., 2013. Tension–torsion fracture experiments–Part II: Simulations with the extended Gurson model and a ductile fracture criterion based on plastic strain. International Journal of Solids and Structures 50.25, 4258-4269.